American Mineralogist, Volume 89, pages 1341–1347, 2004

LETTER

Periodic precipitation pattern formation in hydrothermally treated metamict zircon

THORSTEN GEISLER,[1,*] ANNE-MAGALI SEYDOUX-GUILLAUME,[1,†] MICHAEL WIEDENBECK,[2] RICHARD WIRTH,[2] JASPER BERNDT,[1] MING ZHANG,[3] BORIANA MIHAILOVA,[4] ANDREW PUTNIS,[1] EKHARD K.H. SALJE,[3] AND JOCHEN SCHLÜTER[5]

[1] Institut für Mineralogie, University of Münster, Corrensstrasse 24, D-48149 Münster, Germany
[2] GeoForschungsZentrum Potsdam, Telegrafenberg, D-14473 Potsdam, Germany
[3] Department of Earth Sciences, University of Cambridge, Downing Street, Cambridge CB2 3EQ, U.K.
[4] Institute of Applied Mineralogy, Bulgarian Academy of Science, Rakovski Str. 92, 1000 Sofia, Bulgaria
[5] Mineralogisches Museum, University of Hamburg, Grindelallee 48, D-20146 Hamburg, Germany

ABSTRACT

For more than 100 years mineralogists, physicists, chemists, geologists, and biologists have discussed the formation of periodic Liesegang patterns observed in natural and experimental systems. Spectacular examples of minerals showing complex periodic patterns are agate, malachite, and sphalerite. Here we report the first observation of Liesegang-like patterns in hydrothermally treated metamict (i.e., amorphous) zircon. The structures observed show curved bands, radial sets of pocket-like wave fronts or irregular curved patterns in both cathodoluminescence and backscattered electron images. They are composed of alternating zones of crystallographically well-aligned, polycrystalline zircon along with remnant amorphous pockets and a phase assemblage of randomly oriented zircon crystallites, monoclinic ZrO_2, and amorphous SiO_2, as revealed by transmission electron microscopy. Analyses by secondary ion mass spectrometry and electron microprobe reveal that the latter zones are characterized by higher hydrogen concentrations and higher Zr-Si ratios. Both zones are also distinguishable by a distinctly different crystallite size. We propose a possible pattern-forming mechanism that is based on a feedback of hydrogen diffusion, zircon nucleation, and the displacement of hydrogen atoms from growing crystallites.

INTRODUCTION

The formation of periodic precipitation patterns in the wake of a moving reaction front or interface, known as Liesegang phenomena (Liesegang 1896), is a well known example of spatiotemporal self-organization that has stimulated extensive research for more than a century (Hedges 1932; Henisch 1988). The motivation for these studies comes from the fascination with complex patterns observed in several physicochemical, biological, and geological systems, as well as from the belief that much can be learned about theoretical and practical problems of crystallization processes by investigating the instabilities underlying this phenomenon. The most interesting examples of natural minerals showing Liesegang-like patterns on a macroscopic scale, which have not yet been reproduced experimentally, are agate, sphalerite, and malachite. Experimentally, periodic precipitation has been observed in gelatin and other gels, in porous or granular media like quartz sand, sulfur powder, kieselgur, gypsum, alloys, in gas phases, and even in pure water (e.g., Hedges 1932; Spotz and Hirschfelder 1951; Flicker and Ross 1974; Van Rooijen 1975; Henisch 1988; Senf 1989). Unlike many other pattern-forming systems, such as stationary Turing systems (Turing 1952), the initial conditions are not uniform for Liesegang pattern formation. In a classical Liesegang experiment, periodic precipitation patterns such as rings or bands, depending on the geometry of the system (e.g., Müller et al. 1982; Kuo et al. 1997), emerge behind a propagating wave front when an outer reactant B (e.g., HCl) diffuses into a homogeneous diffusion matrix uniformly filled with a second reactant A (e.g., $AgNO_3$). The role of the diffusion matrix is to prevent convective motion of A and B and the reaction product C (AgCl in the example).

Theoretical models explaining Liesegang patterns fall into two broad categories. The first pre-nucleation model is based on the classical feedback cycle of supersaturation, precipitation, and depletion as originally proposed by Ostwald (Ostwald 1897) and later modeled by various groups (e.g., Dee 1986; Le Van and Ross 1987; Chopard et al. 1994). In the second theory, the so-called post-nucleation or competitive particle growth model, it is assumed that competition between growing particles can, by itself, produce periodic precipitation structures, even in the absence of strong external gradients (e.g., Ortoleva 1982; Feeney et al. 1983; Sultan and Ortoleva 1993). The periodic patterns evolve after the nucleation phase is over through a variant of the Lifshitz-Slyozov instability (Lifshitz and Slyozov 1961). Such a model has been used, for example, to simulate mm-scale Fe-Zn banding in sphalerite (Katsev and L'Heureux 2001).

Here we report the occurrence of diverse periodic precipitation patterns in hydrothermally treated, highly metamict (i.e., amorphous) zircon ($ZrSiO_4$), which further highlight the com-

* E-mail: tgeisler@nwz.uni-muenster.de
† Present address: LMTG, UMR 5563 CNRS, Université Paul Sabatier, 39 allées Jules Guesde, 31000 Toulouse, France

0003-004X/04/0010–1341$05.00

plexity of precipitation pattern formation. The patterns were discovered during an experimental study on the recrystallization behavior of amorphous zircon under various hydrothermal conditions (Geisler et al. 2003a). To our knowledge, these patterns represent the first direct experimental observation of periodic structures formed by a diffusion-reaction process in a dense, although amorphized, silicate mineral.

METHODS

A natural, alluvial zircon sample (HZ7) from Sri Lanka, containing on average 0.62(8) wt% UO_2 and 0.04(1) wt% ThO_2 as determined by electron microprobe, was used in this study (see Geisler et al. 2003a). The sample shows parallel, up to 500 μm wide growth zones in backscattered electron (BSE) images. We were unable to detect any remnant crystalline signals by X-ray diffraction analysis, Raman, infrared, or nuclear magnetic resonance spectroscopies, indicating that the amount of residual crystalline domains is less than ~5%, i.e., that the sample has almost completely been amorphized by high-energy recoil nuclei generated by the U and Th radioactive decay chain over its geological history of about 570 Myr (Gottfried et al. 1956).

We present results from two zircon fragments (nos. 15 and 28) treated under slightly different hydrothermal conditions. Both experiments were carried out at 400 °C in 4 cm long gold tubes filled with small fragments of the zircon sample along with 100 mg of a 0.1N HCl solution. After being welded shut, the gold capsules were placed at the hot spot of a standard cold-seal hydrothermal pressure vessel. The fluid pressure of the experiments with fragments no. 15 and 28 was 100 and 150 MPa and the duration 147 and 51 hours, respectively. The temperature and pressure were constant and accurate within ± 5 °C and ± 5 MPa. After the experiment, the zircon fragments were embedded in Epoxy resin and polished to about half their thickness and then studied by backscattered electron and cathodoluminescence (CL) imaging, micro-Raman spectroscopy, electron microprobe (EMP), secondary ion mass spectrometry (SIMS), as well as by transmission electron microscopy (TEM).

The EMP measurements were carried out with a JEOL JEM 8600 Superprobe. The elements Zr, Si, Hf, Y, P, and U were measured. The operating conditions were 20 keV accelerating voltage at ~100 nA beam current. The lateral resolution for the excitation of Zr$L\alpha$ and Si$K\alpha$ X-rays is better than 4 μm under these conditions. A small chip (500 × 200 μm) of a natural zircon from Sri Lanka (SL-Z2) was used as standard for the Zr, Si, Hf, and U determination. More than 200 electron microprobe analyses were conducted over the last three years to check the homogeneity of the grain and to determine the major and minor element concentration using different standards for Zr, Si, and Hf. The U, Th, and Pb isotopy and chemistry of this zircon grain were repeatedly determined by sensitive high-resolution ion microprobe (for more details see Geisler et al. 2003b).

The TEM investigations were performed with a Philips CM200 TEM and a JEOL 3010 TEM. The JEOL 3010, operating at 300 keV, was used for conventional TEM. The Philips CM200, equipped with an energy-dispersive X-ray analyzer (EDAX) with an ultra-thin window, was used for energy-dispersive X-ray (EDX) analysis and EDX line scans. The acceleration voltage was 200 keV. A focused galium ion beam technique (see, e.g., Seydoux-Guillaume et al. 2003) was used to cut electron transparent slices (~15 μm × 10 μm × 100 nm) perpendicular to the observed structures.

We used the Potsdam Cameca ims 6f SIMS to acquire ^1H point profiles and two-dimensional digital maps. Prior to analysis, the zircon was embedded in the smallest possible volume of Araldite epoxy to minimize the amount of sample outgassing. The polished sample was cleaned and coated with ~35 nm high-purity gold prior to storage overnight in ultra-high vacuum. The total pressure in our secondary source chamber was < $2e^{-9}$ Torr at the time of analysis. The individual analyses employed a 50 pA, nominal 10 kV Cs^+ primary beam, which was focused to a diameter of ~2 μm on the sample surface. Prior to each analysis, an automatic 5 minute pre-burn of the sample was conducted. An actual measurement involved 20 cycles of the peak-stepping sequence 0.95 bkgn (0.1s integration per cycle), $^1H^-$ (10s), $^{28}Si^-$ (2s). Charge compensation employed a normal incidence electron flood gun, which was operated at low power in order minimize the induced hydrogen ion background. The electron-derived background was further suppressed by limiting the field-of-view of our mass spectrometer to a diameter of 30 μm. Our observed background for the $^1H^-$ peak was ~ 500 cps. The mass spectrometer was operated at low mass resolving power M/δM ≈ 600 in conjunction with a 50V energy bandpass with no applied energy offset. Due to the lack of a suitable matrix-matched calibration material, it was not possible to convert our data into absolute hydrogen concentrations.

RESULTS

Figure 1 shows a representative selection of observed structures from the two hydrothermally treated zircon grains, as imaged by the BSE, CL, and X-ray mapping techniques. We note that other experiments carried out at higher fluid temperatures with a 0.1 *N* HCl solution also yielded patterns similar to those shown in Figure 1 and that the external shape of the grains was preserved. The structures observed show (1) radial sets of pocket-like wave fronts, which spread out from the zircon-fluid interface (Fig. 1a) or from cracks (Fig. 1b), (2) equally spaced curved bands (Figs. 1c–f), which were found only in the center of grain no. 28, and (3) irregular and undulatory curved patterns with complex branching effects (Figs. 1g–i). The equally spaced banding structure gradually fades into the irregular pattern (Figs. 1e and 1f). The structures are formed by 1-2 μm bands or zones (labeled "A" in Fig. 1), which appear brighter in the BSE and CL images. These zones or bands alternate with usually larger regions (labeled "B" in Fig. 1), which are characterized by lower BSE and CL intensities (compare Fig. 1c and d). The structures shown in Figures 1a and b have striking similarities with those observed in a geometrically inverted Liesegang experiment when the outer reactant diffuses toward the center of a circular gel section placed in a petri dish (Müller et al. 1982). Furthermore, the spacing between the A regions increases away from the zircon-fluid interface as observed in classical Liesegang experiments. This behavior is predicted by the spacing law, which states that the ratio of the position of two consecutive bands x_n and x_{n+1} (starting from an arbitrary point) approaches a constant value p as the number of bands increases (Jablczynski 1923), i.e., $x_{n+1}/x_n = p$. The observed value for p for the wave fronts shown in Figure 1a is 1.09(2) (Fig. 2) and thus falls well within the range of p's found in both experimental and numerical studies (typically $1.05 \leq p \leq 1.15$, Chopard et al. 1994), suggesting some mechanistic similarities with classical Liesegang systems. However, we note that the bands shown in Figures 1c-f are equally spaced, i.e., yield a p of 1.00(1) (Fig. 2).

Since the BSE intensity depends on the mean atomic number of the target material, the BSE contrast between regions A and B in Figure 1 implies that the two zones have different chemical compositions. Indeed, quantitative EMP measurements reveal that the B regions have the highest Zr-Si weight ratios, whereas the A bands have Zr-Si ratios close to those observed in the starting material (Fig. 3). Zr distribution maps also show that the B regions have higher absolute Zr concentrations (Fig. 1h). SIMS point profiles (Fig. 3a) and two-dimensional hydrogen maps (inset diagram of Fig. 1b) further document striking variations in the total hydrogen content. The SIMS data reveal that there is a trend to higher hydrogen concentrations in those regions giving the lowest BSE intensity, the highest Zr/Si weight ratios, and the lowest Si concentrations, i.e., in the B regions. The higher hydrogen and the lower Si concentration in the B regions are consistent with the significant lower BSE intensity generated from these areas.

Figure 4 shows representative TEM bright-field (BF) images and selected area electron diffraction patterns (SAED) for the A and B regions. Two regions of different crystallite size are distinguishable in BF images (Fig. 4a), which correspond to regions A and B, respectively. Region A consists mainly of polycrystalline

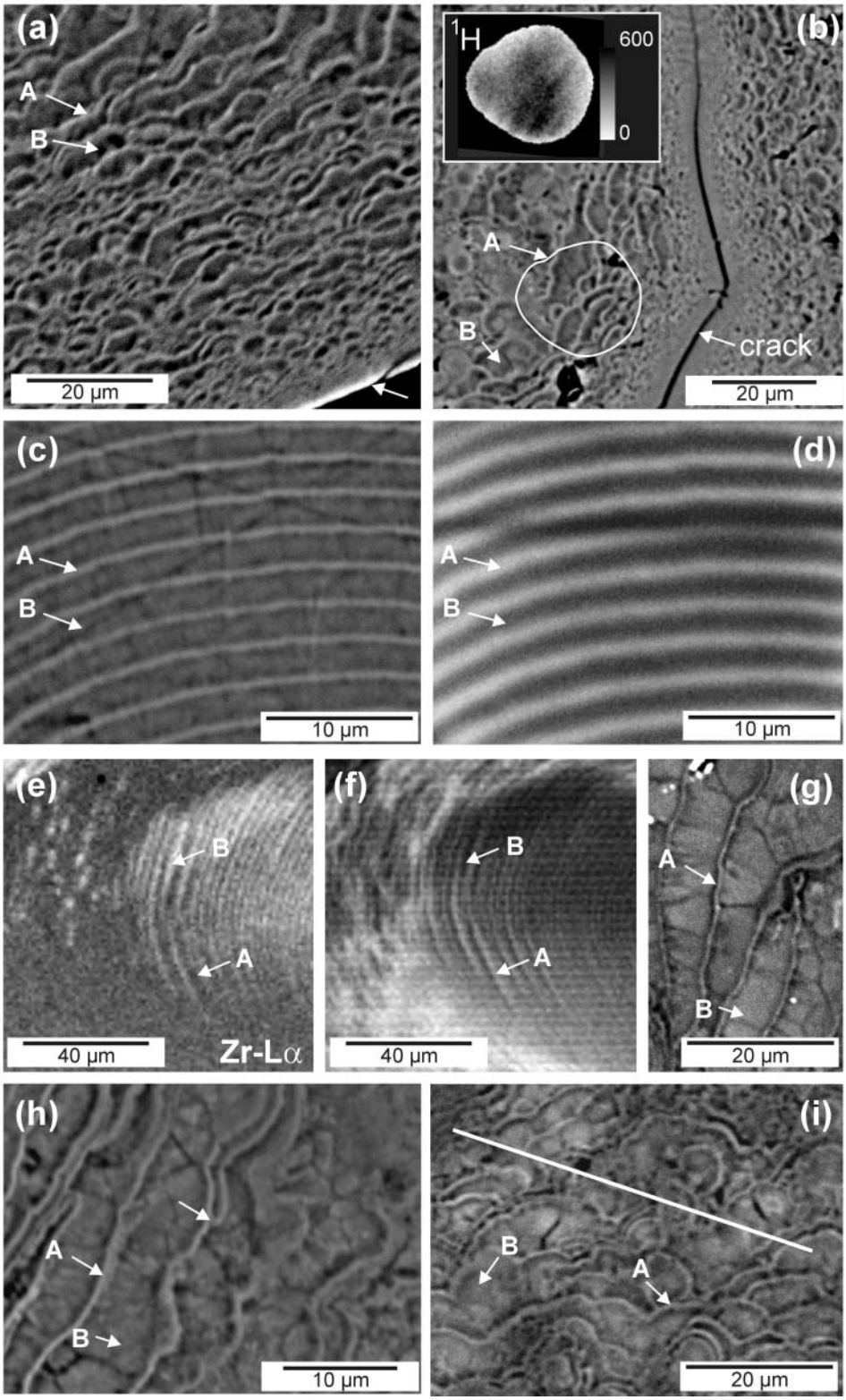

FIGURE 1. (**a-c**, **g-i**) BSE and (**d**, **f**) CL images, and (**e**) a Zr*L*α intensity map of hydrothermally treated metamict zircon. Inset in **b** is a SIMS hydrogen distribution map of the region outlined by the white circle in the BSE image. Note that the highest hydrogen signal is shown in black to allow a direct comparison with the BSE image. The white margin in the image is an analytical artifact. White arrows mark regions A and B (see Table 1). The unlabeled white arrow in **a** points to the original zircon-fluid interface and in **h** to a bifurcation point. The white line in **i** marks the position of the SIMS and electron microprobe point profile shown in Figure 3. Note that secondary electron images show that the surfaces of the grains are flat.

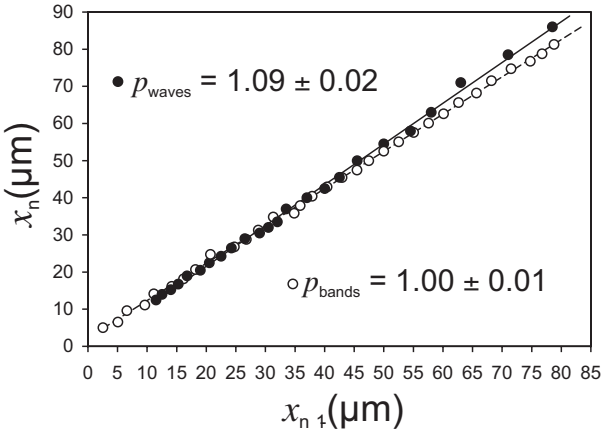

FIGURE 2. The spacing of consecutive bands of the structure shown in Figure 1a (p_{waves}) and Figures 1c and d (p_{bands}).

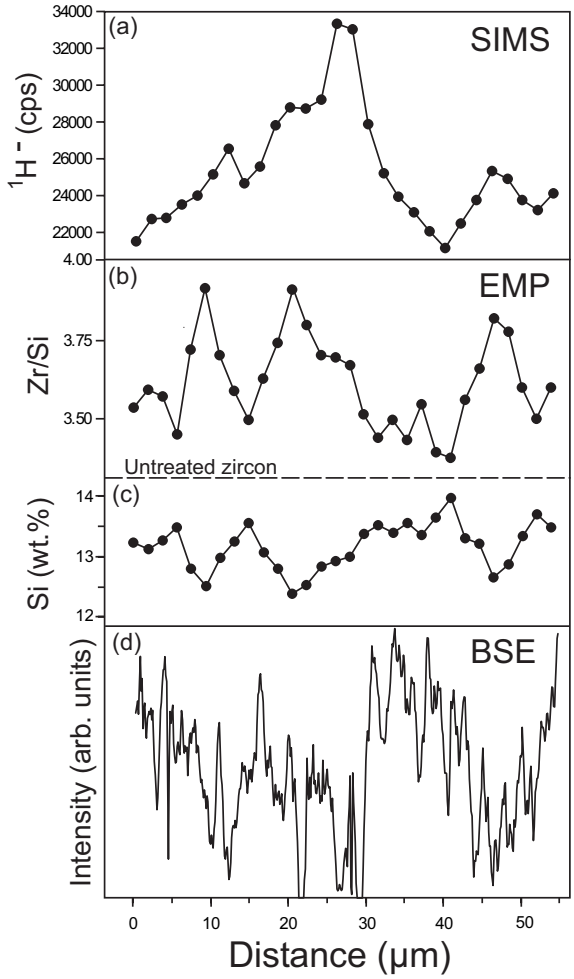

FIGURE 3. The spatial correlation between (**a**) SIMS hydrogen secondary ions signals, (**b**, **c**) electron microprobe data, and (**d**) the BSE intensity, extracted from the corresponding BSE image. The location of the line profile is marked by a white line in Figure 1i. The 2σ counting errors are within the size of the symbols. Note that a perfect correlation between the electron and ion microprobe profile and the BSE intensity is not expected since these techniques probe significantly different depth volumes.

zircon and amorphous zircon remnants, as revealed by the BF images (Fig. 4b) and SAED patterns (Fig. 4c). The occurrence of isolated diffraction spots is usually typical for single-crystal diffraction patterns. Such a pattern indicates that the zircon crystallites shown in the BF images are crystallographically well-oriented (Fig. 4c and 4d). The zircon grains are organized in a high energy, non-equilibrium texture with quadruple junctions (Fig. 4b). This unusual nano-scale texture contrasts with the polygonal equilibrium texture of random oriented zircon crystallites formed during dry annealing experiments in highly radiation-damaged, amorphous zircon (Capitani et al. 2000). It implies that the crystallographic information is transferred between successively nucleated particles, i.e., that nucleation at the reaction front must have occurred on grain boundaries or surfaces of previously nucleated crystallites. The B regions, on the other hand, are composed of randomly oriented zircon crystallites, as seen in the BF images and as polycrystalline rings in the SAED patterns (Figs. 4f and 4g). We note, however, that the additional occurrence of "bean-shaped" diffraction spots indicates a preferred crystallographic orientation of some zircon crystallites, which is identical to the orientation of the zircon crystallites of region A (compare the SAED patterns shown in Figs. 4c and 4f, which were made under the same diffraction conditions). This observation suggests that two zircon generations are present within the B regions. Furthermore, monoclinic ZrO_2 crystallites and amorphous SiO_2 (see Fig. 3a) could also be detected in areas within the B regions by electron diffraction and energy-dispersive X-ray (EDX) microanalysis. The ZrO_2 crystallites are mostly oriented randomly, but some show orientation preference (Fig. 4g). The occurrence of monoclinic ZrO_2 in the B regions and their absence in the A regions could also be verified by micro-Raman spectroscopy. The physicochemical characteristics of both regions are summarized in Table 1.

A striking feature of the BF images is the occurrence of bright areas, which are particularly obvious within the A regions (Fig. 4a). EDX analyses revealed that the Zr and Si X-ray intensity ratio in these areas is identical to that of the dark areas, but with lower absolute intensities (Fig. 4a). Consequently, the bright areas cannot be attributed to diffraction contrast, but rather must reflect thinner regions. These regions most likely represent nano-sized pores, which are a consequence of the amorphous-to-crystalline transition because crystalline zircon has a 18% lower molar volume than amorphous zircon (Holland and Gottfried 1955). Such a nano-porous structure allows fast chemical transport to and from the reaction front, such that the rate-determining step is the process occurring at the interface. This porous structure is probably responsible for the milky-white optical appearance of radiation-damaged zircon after hydrothermal treatment in this experiment and others (Geisler et al. 2003a, 2003b, 2003c).

DISCUSSION

Although the observed recrystallization patterns have remarkable similarities with Liesegang patterns, the system investigated here is different from a classical Liesegang system, which involves a chemical reaction of the form A + B → C within a gel. The observed strong recrystallization at 400 °C is surprising when compared with the high temperatures needed to recrystallize amorphous zircon under dry conditions (e.g., Zhang et al.

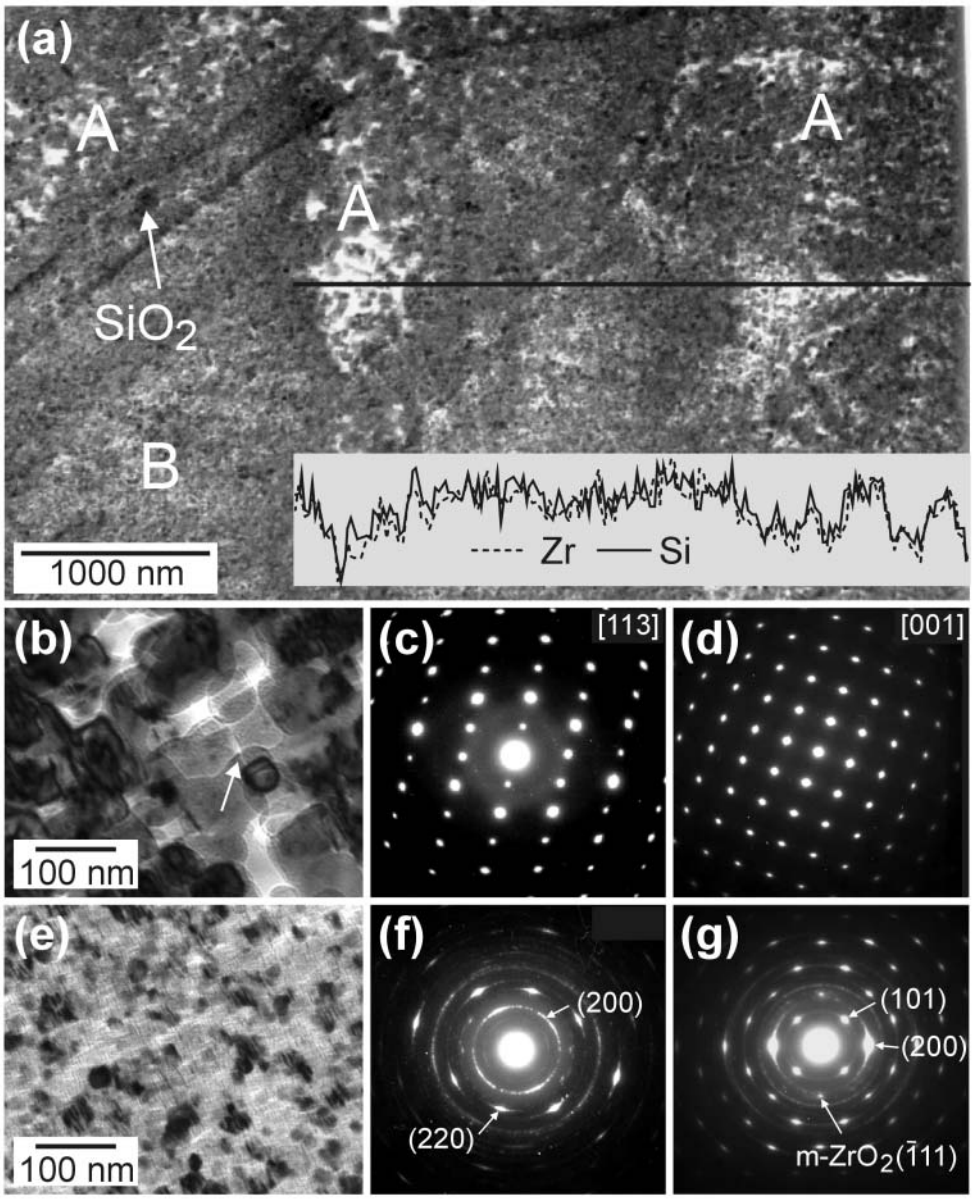

FIGURE 4. Bright field (BF) images and selected area electron diffraction (SAED) patterns of hydrothermally treated, metamict zircon. (**a**) BF image (EDX scanning mode) showing the spatial arrangement of the A and B regions in the third dimension. Those areas with white BF contrast are characterized by a lower X-ray intensity of Zr and Si, as revealed by an energy dispersive X-ray line scan along the black line. These areas most likely represent nano-sized pores, caused by the 18% volume reduction during the amorphous-to-crystalline transition. (**b**) BF image of the A region. The white arrow points to a high energy, non-equilibrium grain boundary configuration. (**c**) SAED pattern of the A region shown in **b** with diffuse rings from amorphous remnants. (**d**) SAED pattern of the A region without diffuse rings. The diffraction pattern shows that the crystallites are crystallographically well-oriented. (**e**) BF image of the B region (**f**) SAED pattern of the B region shown in **e**, obtained with the same sample orientation as the pattern shown in **c**. Note that the zircon grains are randomly oriented, but with a preferred orientation that is the same as in the A regions [compare with the SAED pattern in (**c**)] (**g**) SAED pattern of the B region with diffraction signals from monoclinic ZrO_2.

TABLE 1. Physicochemical characteristics of the structure forming regions

Region/ Band	BSE intensity	CL intensity	Hydrogen concentration	Zr/Si ratio	Phase assemblage	Cryst. orientation	Grain size (nm)
A	high	high	low	low	crystalline $ZrSiO_4$	oriented	~50–200
					amorphous $ZrSiO_4$	_	
B	low	low	high	high	crystalline $ZrSiO_4$	random*	~20–50
					monoclinic ZrO_2	random*	
					amorphous SiO_2	_	

* Some crystals show a preferred orientation.

2000; Geisler 2002). This observation, however, confirms previous experimental results and shows that the activation energy for recrystallization is greatly reduced in hydrothermal environments (Geisler et al. 2003a, 2003b). This fact suggests that the patterns formed during the amorphous-to-crystalline transition, which is driven by the inward diffusion of hydrogen. Hydrogen may occur as either H^+ and/or likely as molecular water (Geisler et al. 2003a, 2003b, 2003c; unpublished data). There is experimental evidence that in highly radiation-damaged zircon crystals, such as the one used in our experiments, bulk hydrogen diffusion is dramatically enhanced by interconnected nano-sized, amorphous regions of a lower atomic density which act as high-diffusivity pathways (Geisler et al. 2003c; Ríos and Salje 2004). Such low-density regions are produced by high-energy recoil nuclei generated during the radioactive decay of U and Th, as seen in molecular-dynamics simulations (Trachenko et al. 2002; Geisler et al. 2003c). The reduction of the activation energy of recrystallization in a hydrothermal environment may be understood when considering that the rate of zircon nucleation is increased via the formation of intermediate OH species by the hydrolysis of Si-O-Si bonds of the amorphous network. Such depolymerization reactions increase the mobility of the network-forming atoms and thus also the overall nucleation rate, i.e., they reduce the activation energy of self-diffusion. This interpretation is supported by a recent first-principle simulation of the diffusion of water in amorphous SiO_2, which has shown that the formation energy of silanol (Si-OH) is lower than the energy needed for a water molecule to freely diffuse when the network consists of five-membered or smaller rings (Bakos et al. 2002). We also note that infrared spectroscopic evidence for the existence of new OH species (which may be related to silanol groups) in the reacted amorphous network has been recently presented (Geisler et al. 2003a).

The observation that zircon crystallites have nucleated inside both A and B regions indicate that the pattern evolves after nucleation has already started. The different crystallite size suggests, at first glance, an Ostwald ripening mechanism. However, pattern formation through ripening requires long-range feedback based on diffusion of the chemical components of the precipitates, resulting in the dissolution of smaller grains, which are located the diffusion distance away from the initial growth perturbation (e.g., Feeney et al. 1983). Such long-range diffusion is not necessary in the course of the amorphous-to-crystalline transition. Note, however, that feedback is necessary for the development of a pattern from an unpatterned state (Nicolis and Prigogine 1977). Apart from the fact that hydrogen acts as an "activator" for the transformation process, it may also be responsible for the pattern-forming feedback, i.e., for the "inhibition" of continuous zircon growth behind the front. A possible feedback mechanism is suggested by the fact that the zircon lattice can structurally incorporate only a limited amount of hydroxyl (e.g., Woodhead et al. 1991). We notice that infrared measurements of powder of the same sample treated under the same conditions have shown that some hydrogen is sited in crystalline domains but that most is located in an amorphous environment (Geisler et al. 2003a). We propose that an initially unpatterned state behind the reaction front, consisting of crystallographically oriented, i.e., epitaxially grown zircon crystallites and remnant amorphous domains, becomes unstable due to a perturbation that is induced by the displacement of excess hydrogen from the growing zircon crystallites. The growth of the zircon crystallites generates an increase in the hydrogen concentration in the surrounding amorphous regions. The internal hydrogen gradient must lead to diffusion of the expulsed hydrogen in the direction of the moving reaction front, resulting in a secondary hydrogen diffusion front, which lags somewhat behind the main reaction front. We further hypothesize that the increase in the hydrogen concentration drives the amorphous phase further away from thermodynamic equilibrium (analogous to the effect of an increasing undercooling of a melt) and further increases the mobility of the network-forming atoms (in contrast to the effect of an increasing undercooling of a melt). This may lead to a dramatic increase in the nucleation rate within the remnant amorphous domains once a threshold hydrogen concentration has been reached. We suggest that such nucleation events formed the randomly oriented crystallites in the B region (Fig. 4f). Further nucleation and growth of zircon, however, further increases the hydrogen concentration in the amorphous relicts, which may now occur as isolated pockets. Eventually, a situation may be reached where it is energetically more advantageous to form a metastable assemblage of monoclinic ZrO_2 and amorphous SiO_2, i.e., to decompose amorphous zircon rather than to allow zircon nucleation and growth. The amorphous SiO_2 seen in Figure 4a may now act as a local sink for hydrogen. The higher Zr-Si ratios observed in the B regions may indicate that some of the silica has been selectively removed from the system since silica has a significantly higher solubility than zirconia in acidic aqueous solutions (Tole 1985). Close behind the main reaction front the zircon crystallites can freely grow since they are not affected by the secondary hydrogen front. However, as they grow, they expel more and more hydrogen, again producing a new hydrogen front that induces rapid nucleation and decomposition of zircon. The repetitive generation of secondary hydrogen fronts behind the main reaction front leads to the formation of alternating zones of crystallographically well-aligned zircon crystallites with remnant amorphous pockets and a phase assemblage of randomly oriented polycrystalline zircon, monoclinic ZrO_2 crystallites, and hydrogen-rich, amorphous SiO_2.

Although Liesegang phenomena have been known for more than 100 years, the mechanisms underlying their formation remain controversial. What we can add to the discussion is the occurrence of complex Liesegang-like patterns formed during the recrystallization of a radiation-damaged, amorphous material that is unique with respect to the occurrence of nano-scale density fluctuations. It must be these density fluctuations, which permit hydrogen diffusion to be faster than dissolution (and recrystallization) of amorphous zircon. A possible qualitative diffusion-reaction mechanism for the formation of the observed patterns is based on the feedback of hydrogen diffusion, zircon nucleation, and the displacement of hydrogen from growing crystallites. We note that hydrothermal treatment of the same sample at 600 °C and 100 MPa fluid pressure in a 2 *M* $CaCl_2$ solution, for example, did not produce rhythmic patterns (Geisler et al. 2003c), whereas localized curved banding patterns have been observed in a partially metamict sample treated under similar conditions (Geisler et al. 2003b). It thus seems likely that such patterns will

only evolve when a fine balance exists between the velocity of the hydrogen diffusion front, partly determined by the degree of amorphization (Geisler et al. 2003b), and the nucleation and growth kinetics. In this context, it is interesting to note that—although rarely documented in the literature (e.g., Pidgeon et al. 1998)—secondary, non-equilibrium internal banding in zircon appears to be a common feature in nature, as indicated by the frequent occurrence of curved banding in detrital zircon populations of quartzites from the Eckergneiss Complex in the Harz Mountains, Germany (Geisler et al., in preparation). However, although it is very likely that these structures were also formed by a diffusion-reaction process, it is currently unknown whether the mechanism that has produced banding structures in nature is identical or similar to the one that created the experimental patterns. Future research should involve a quantitative treatment of the problem to evaluate, if—respectively under which circumstances—the proposed mechanism is able to produce the experimentally observed as well as the natural patterns.

ACKNOWLEDGMENTS

Many thanks go to B. Cornelisen and D. Gebauer for their help with the cathodoluminescence investigations. The manuscript has strongly benefited from many fruitful discussions with K. Pollok. We would also like to thank A. Meldrum and an anonymous reviewer for their helpful comments.

REFERENCES CITED

Bakos, T., Rashkeev, S.N., and Pantelides, S.T. (2002) Reaction and diffusion of water and oxygen molecules in amorphous SiO_2. Physical Review Letters, 88, 055508(4).

Capitani, G.C., Leroux, H., Doukhan, J.C., Ríos, S., Zhang, M., and Salje, E.K.H. (2000) A TEM investigation of natural metamict zircons: structure and recovery of amorphous domains. Physics and Chemistry of Minerals, 27, 545–556.

Chopard, B., Luthi, P., and Droz, M. (1997) Reaction-diffusion cellular automata model for the formation of Liesegang patterns. Physical Review Letters, 72, 1384–1387.

Dee, G.T. (1986) Patterns produced by precipitation at a moving reaction front. Physical Review Letters, 57, 275–278.

Feeney, R., Schmidt, S.L., Strickholm, P., Chadam, J., and Ortoleva, P. (1983) Periodic precipitation and coarsening waves: Application of the competitive particle growth model. Journal of Chemical Physics, 78, 1293–1311.

Flicker, M. and Ross, J. (1974) Mechanism of chemical instability for periodic precipitation. Journal of Physical Chemistry, 60, 3485–3456.

Geisler, T. (2002) Isothermal annealing of partially metamict zircon: evidence for a three-stage recovery process. Physics and Chemistry of Minerals, 29, 420–429.

Geisler, T., Zhang, M., and Salje, E.K.H. (2003a) Recrystallization of almost fully amorphous zircon under hydrothermal conditions: An infrared spectroscopic study. Journal of Nuclear Materials, 320, 280–291.

Geisler, T., Pidgeon, R.T., Kurtz, R., van Bronswijk, W., and Schleicher, H. (2003b) Experimental hydrothermal alteration of partially metamict zircon. American Mineralogist, 86, 1496–1513.

Geisler, T., Trachenko, K., Ríos, S., Dove, M.T., and Salje, E.K.H. (2003c) Impact of self-irradiation damage on the aqueous durability of zircon ($ZrSiO_4$): Implications for its suitability as nuclear waste form. Journal of Physics: Condensed Matter, 15, L597–L605.

Gottfried, D., Senftle, F.E., and Waring, C.L. (1956) Age determination of zircon crystals from Ceylon. American Mineralogist, 41, 749–765

Hedges, E.S. (1932) Liesegang rings and other periodic structures. Chapman and Hall, London.

Henisch, H.K. (1988) Chrystals in gels and Liesegang rings. Cambridge University Press, Cambridge.

Holland, H.D. and Gottfried D. (1955) The effect of nuclear radiation on the structure of zircon. Acta Crystallographica, 8, 291–300.

Jablczynski, K. (1923) Memoires presentes à la société chimique. Les anneaux de Liesegang. Bulletin Société Chimie de France, 33, 1592–1602.

Katsev, S. and L'Heureux, I. (2001) Two-dimensional model of banding pattern formation in minerals by means of coarsening waves: Mississippi Valley-type sphalerite. Physics Letters A, 292, 66–74.

Kuo, C.-S., Cabaracos, E.L., and Bansil, R. (1997) Two-dimensional pattern formation in reaction-diffusion systems. Influence of the geometry, Physica A, 239, 120–128.

Le Van, M.E. and Ross, J. (1987) Measurements and hypothesis on periodic precipitation processes. Journal of Physical Chemistry, 91, 6300–6308.

Liesegang, R.E. (1896) Über einige Eigenschaften von Gallerten. Naturwissenschaftliche Wochenschriften, 11, 353–362.

Lifshitz, I.M. and Slyozov, V.V. (1961) The kinetics of precipitation from supersaturated solid solutions. Journal of Physical Chemistry of Solids, 19, 35–50.

Müller, S.C., Kai, S., and Ross, J. (1982) Curiosities in periodic precipitation patterns. Science, 216, 635–637.

Nicolis, G. and Prigogine, I. (1977) Self-organization in nonequilibrium systems. John Wiley and Sons.

Ortoleva, P.J. (1982) Solute reaction mediated precipitate patterns in cross gradient free systems. Zeitschrift für Physik B: Condensed Matter, 49, 149–156.

Ostwald, W. (1897) A-Linien von R.E. Liesegang (review). Zeitschrift für Physikalische Chemie, 23, 356.

Pidgeon, R.T., Nemchin, A.A., and Hitchen, G.J. (1998) Internal structures of zircons from Archean granites from the Darling Range batholith: implications for zircon stability and the interpretation of zircon U-Pb ages. Contributions to Mineralogy and Petrology, 132, 288–299.

Ríos, S. and Salje, E.K.H. (2004) Density fluctuations in self-irradiated zircon. Applied Physics Letters, 84, 2061–2063.

Senf, L. (1989) Rythmic precipitation (Liesegang rings) in gases. Zeitschrift für Physikalische Chemie, 270, 1020–1022.

Seydoux-Guillaume, A.-M., Goncalves, P., Wirth, R., and Deutsch, A. (2003) Transmission electron microscope study of polyphase and discordant monazites: Site-specific specimen preparation using the focused ion beam technique. Geology, 31, 973–976.

Spotz, E.L. and Hirschfelder, J.O. (1951) Liesegang ring formation arising from diffusion in ammonia and hydrogen chlorine gases through air. Journal of Chemical Physics, 19, 1215–1219.

Sultan, R. and Ortoleva, P. (1993) Periodic and aperiodic patterning in two precipitate post-nucleation systems. Physica D, 63, 202–212.

Tole, M.P. (1985) The kinetics of dissolution of zircon ($ZrSiO_4$). Geochimica Cosmochimica Acta, 49, 453–458.

Trachenko, K., Dove, M., and Salje, E.K.H. (2002) Structural changes in zircon under α-decay irradiation. Physical Review B, 65, 180102 (R).

Turing, A. (1952) The chemical basis of morphogenesis. Philosophical Transaction Royal Society of London, Series B, 237, 37–72.

Van Rooijen, V.A., van Royen, E.W., Vrijen, J., and Radelaar, S. (1975) On Liesegang bands in internally oxidized AgCd-based ternary alloys. Acta Metallica, 23, 987–995.

Woodhead, J.A., Rossman, G.R., and Silver, L.T. (1991) Hydrous species in zircon. American Mineralogist, 76, 1533–1546.

Zhang, M., Salje, E.K.H., Farnan, I., Capitani, G.C., Leroux, H., Clark, A.M., Schlüter, J., and Ewing, R.C. (2000) Annealing of α-decay damage in zircon: a Raman spectroscopic study. Journal of Physics: Condensed Matter, 12, 3131–3148.

MANUSCRIPT RECEIVED JANUARY 8, 2004
MANUSCRIPT ACCEPTED MARCH 22, 2004
MANUSCRIPT HANDLED BY LEE GROAT